Dynamic Implications of Non-Covalent Interactions in Amphiphilic Single-Chain Polymer Nanoparticles

Peter A. Dykeman-Bermingham[†a], Laura R. Stingaciu[‡a], Changwoo Do[‡], Abigail S. Knight[†,*]

†Department of Chemistry, The University of North Carolina at Chapel Hill, Chapel Hill, North Carolina, 27599, United States

‡NScD, SNS, Oak Ridge National Laboratory, Oak Ridge National Laboratory, Oak Ridge, Tennessee, 37830, United States

Abstract: Single-chain polymer nanoparticles (SCNPs) combine the chemical diversity of synthetic polymers with the intricate structure of biopolymers, generating versatile biomimetic materials. The mobility of polymer chain segments at length scales similar to secondary structural elements in proteins are critical to SCNP structure and thus function. However, the influence of non-covalent interactions used to form SCNPs (e.g., hydrogen-bonding and biomimetic secondary-like structure) on these conformational dynamics is challenging to quantitatively assess. To isolate the effects of non-covalent interactions on SCNP structure and conformational dynamics, we synthesized a series of amphiphilic copolymers containing dimethylacrylamide and monomers capable of forming these different interactions: 1) di(phenylalanine) acrylamide that forms intramolecular β-sheet-like crosslinks, 2) phenylalanine acrylamide that forms hydrogen-bonds, but lacks a defined local structure, and 3) benzyl acrylamide that has lowest propensity for hydrogen-bonding. Each SCNP formed folded structures comparable to those of intrinsically disordered proteins, as observed by size exclusion chromatography and Small Angle Neutron Scattering. The dynamics of these polymers, as characterized by a combination of dynamic light scattering and Neutron Spin Echo spectroscopy, was well described using the Zimm with internal friction (ZIF) model, highlighting the role of each non-covalent interaction to additively restrict the internal relaxations of SCNPs. These results demonstrate the utility of local scale interactions to control SCNP polymer dynamics, guiding the design of functional biomimetic materials with refined binding sites and tunable kinetics.

Introduction

Single-chain polymer nanoparticles (SCNPs) are folded synthetic macromolecules that resemble biopolymers, such as intrinsically disordered proteins, in their size and flexibility.[1–3] Numerous strategies can direct polymer folding, including non-covalent[4,5] and covalent[6–8] interactions, in addition to metal coordination.[9–11] This creates a tunable platform for diverse functions including catalysis and binding target molecules.[12–14] Leveraging this synthetic versatility, variations to the composition and structure of SCNPs have been effectively employed to improve their functional performance.[15–18] In most cases, the evaluation of polymer structure-activity relationships relies on time averaged analyses, such as size exclusion chromatography and multi angle light scattering, which obscure conformational dynamics that are faster than the acquisition time (on the order of seconds).[19] However, there is a growing appreciation that conformational dynamics (e.g. center of mass diffusion and segmental relaxations) of soft materials, including SCNPs and proteins, mediate or are altered by their functions.[13,20] Therefore, time-resolved structural information is required to develop comprehensive structure-function relationships.

These conformational dynamic modes on time scales relevant to polymer functions (ps-ns) are observable with both small-angle scattering and NMR techniques.[13,20–22] Analyses connecting static structures with chain dynamics using these techniques have highlighted that both hydrophobicity and covalent crosslinking dampen SCNP mobility.[7,23,24] Neutron Spin Echo spectroscopy (NSE) offers spatial and temporal resolution, uniquely enabling the assessment of polymer dynamics at length scales relevant to local, secondary-like, structure. The underlying mechanisms of these measurements are interpretable through analyses derived from polymer theory. For example, internal friction, which encompasses energetic barriers to chain relaxation (e.g., intrachain collisions and hydrogen bonding), has been implicated in the dynamics of intrinsically disordered proteins,[25,26] polyelectrolytes,[27] and covalently folded SCNPs in dilute solution.[28,29] While the impact of hydrophobic collapse and covalent crosslinks on chain dynamics is established, it remains unclear how noncovalent interactions that generate local structure restrict the chain dynamics of dilute SCNPs.

We recently reported a di(phenylalanine) acrylamide (FF) monomer that facilitates the folding of amphiphilic copolymers through both hydrophobic collapse and local-scale β-sheet-like interactions that provides an ideal model system to correlate local non-covalent interactions to internal friction.[30] We observed that FF-based SCNPs formed similar global (nm length scale) structures to analogous phenylalanine acrylamide (F)- and *N*-benzyl acrylamide (BAA)-containing copolymers; however, FF-copolymers provided unique local rigidity. In this work, we report the static and dynamic structures of amphiphilic SCNPs containing FF, F, and BAA as observed by Small Angle Neutron Scattering and NSE. We identified additive contributions of non-covalent interactions including hydrogen-bonding and β-sheet-like local structure to internal friction, which restricts chain mobility. These results illustrate the role of local scale structures to mediate polymer dynamics towards complex functionality.

Results and Discussion

To isolate the effects of non-covalent interactions on the structure and dynamics of single-chain polymer nanoparticles (SCNPs), a series of amphiphilic copolymers were synthesized. An inert hydrophilic comonomer, dimethylacrylamide (DMA), was selected to ensure intramolecular interactions were dominated by the hydrophobic moiety. The hydrophobic comonomers – di(phenylalanine) acrylamide (FF), phenylalanine acrylamide (F), and *N*-benzyl acrylamide (BAA) – were chosen to systematically screen intramolecular interactions and thus local structure complexity (Figure 1a).[30] Each motif is capable of both hydrophobic and aromatic interactions; however, FF and F have greater propensities for forming hydrogen bonds than BAA, and FF uniquely forms intramolecular β-sheet-like fibrils.

Three SCNPs, copolymers of each hydrophobic monomer with DMA, were synthesized via reversible addition-fragmentation transfer (RAFT) polymerization to yield chains with similar molecular weights (~ 12 kDa) and with low molecular weight dispersity (< 1.2; Figure 1b and Tables S1-2). To achieve similar degrees of global collapse while maintaining solubility in aqueous solution at high concentrations, each copolymer included approximately 20 wt% of the hydrophobic monomer.[30,31] A homopolymer of DMA (pDMA) was also synthesized at the same molecular weight to estimate the dynamic contributions of the SCNP segments composed of solely DMA.

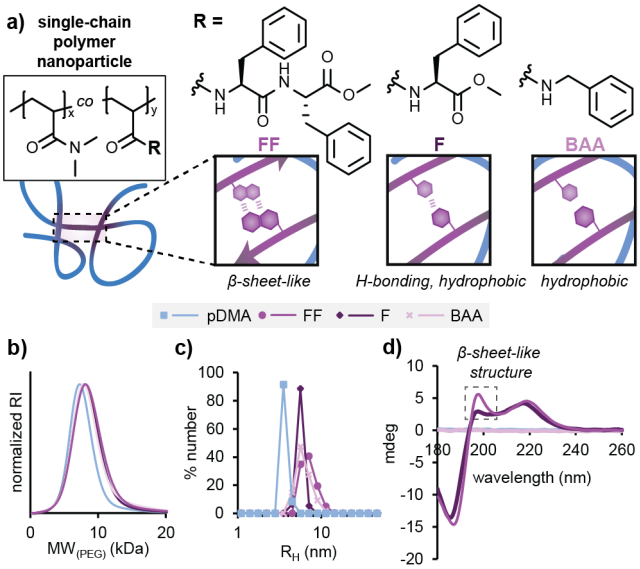

Figure 1. Time-averaged structural characterization of model polymers. a) Schematic of single-chain polymer nanoparticles (SCNPs) with different non-covalent interactions. b) Size exclusion chromatograms (DMF) of SCNPs and pDMA. Molecular weight axis was calculated relative to PEG standards. c) Dynamic light scattering distributions of polymer radii of hydration (30 mg/mL, deuterated phosphate buffer). d) Circular dichroism spectra of SCNPs and pDMA (0.2 mg/mL, deuterated phosphate buffer).

Neutron scattering techniques, including Small Angle Neutron Scattering (SANS) and Neutron Spin Echo spectroscopy (NSE), are unparallelled for characterizing the static and dynamic structures of polymer and protein materials at length and time scales relevant to their functions.[22,32] To elicit high scattering contrast in these scattering experiments, the labile amide protons in the copolymers were exchanged in deuteroxide and stored as a lyophilized powder prior to dissolution in deuterated buffer for analysis. To ensure consistent solvent viscosity and hydrogen-bond strength, aqueous polymer samples were similarly prepared in deuterated buffer.

Polymer conformation was first observed by dynamic light scattering (DLS; 10 mM phosphate buffer pH 7, redissolved in D_2O). Consistent with previous observations in aqueous solution, each polymer formed predominantly single chain assemblies ($R_H < 10$ nm; Figures 1c and S1).[30] The single-chain morphologies were corroborated with aqueous phase size exclusion chromatography (0.1 M sodium phosphate buffer, pH 7.0, natural isotopic abundance), which further demonstrated that SCNPs were more compact the pDMA, as previously observed (Figure S2).[30] The structure of SCNPs at shorter length scales, akin to secondary structure, was observed by circular dichroism (CD; 1 mM sodium phosphate pH 7, redissolved in D_2O; Figures 1d and S3). The FF-DMA copolymer exhibited a pronounced maximum at 198 nm associated with intramolecular β-sheet-like interactions.[17,30,33] This feature was weaker for F-DMA, demonstrating a less defined local structure. No CD response was observed for BAA-DMA or pDMA, which do not have a controlled chiral structure.[30] We thus hypothesized that the difference in local structure between FF-, F-, and BAA-DMA copolymers would mediate the mobility of polymer segments.

The interpretation of SCNP and pDMA dynamics measured by NSE requires quantitative descriptions of the time-averaged structure of these polymers, accessible with SANS. SANS experiments were performed on the Extended Q-Range Small-Angle Neutron Scattering Diffractometer, EQ-SANS, BL-6, SNS at Oak Ridge National Laboratory.[34] The polymer morphology was first observed qualitatively by visualizing the scattering profiles in the dimensionless Kratky projection [Figure 2a; $(qR_g)^2I(q)/I(0)$ vs. qR_g where q is the momentum, R_g is the radius of gyration, and $I(q)/I(0)$ is the normalized scattering intensity].[35] In this projection, a characteristic bell shape is indicative of a globular morphology (as in lysozyme) and a perpetual positive slope is characteristic of intrinsically disordered proteins (IDP; i.e. adenovirus early gene 1A protein).[35–38] The SCNPs resemble the global morphology of the representative IDP, as the slope decreases after $qR_g = 2$, consistent with previous reports of SCNPs.[1,39,40] The influence of the hydrophobic monomers to form folded morphologies is evident when comparing SCNPs to pDMA, as pDMA resembles a random coil in the same conditions.[35] Careful inspection of FF-DMA in this projection reveals an inflection to a negative slope, indicating a more densely folded structure as compared to the analogous F- and BAA-DMA copolymers. This observation that FF-DMA is more folded than F- and BAA-DMA, which contain approximately double the number of hydrophobic monomers, highlights the strength of the local structural interactions to influence global morphology.

Quantitative descriptions of polymer structure are critical for analysis of polymer dynamics. Calculations of the R_g, intensity at zero scattering angle [I(0)], the scaling exponent (ν), and the form factor [P(q), calculated at 2.5 mg/mL] for each polymer were performed

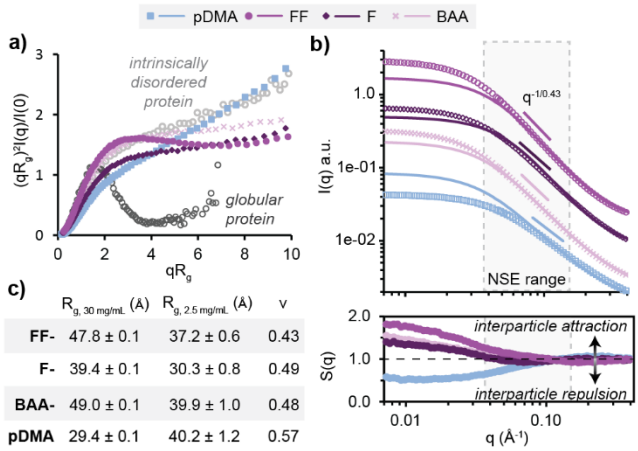

	$R_{g,\ 30\ mg/mL}$ (Å)	$R_{g,\ 2.5\ mg/mL}$ (Å)	ν
FF-	47.8 ± 0.1	37.2 ± 0.6	0.43
F-	39.4 ± 0.1	30.3 ± 0.8	0.49
BAA-	49.0 ± 0.1	39.9 ± 1.0	0.48
pDMA	29.4 ± 0.1	40.2 ± 1.2	0.57

Figure 2. Small Angle Neutron Scattering (SANS) analysis of single-chain polymer nanoparticles (SCNPs) and pDMA. a) Dimensionless Kratky projection of polymers and model proteins. Small Angle X-ray Scattering spectrum for intrinsically disordered protein, adenovirus early gene 1A protein, was thinned to include 1 of 10 datapoints for clarity.[36] SANS spectrum for model globular protein, lysozyme, was reproduced without change.[35] b) Scattering profile (top) and structure factor (bottom) of polymers. Open symbols are intensities at 30 mg/mL and lines are form factor fits at 2.5 mg/mL. Data are y-axis scaled for clarity. Bars indicate q range observed by Neutron Spin Echo experiments. c) Calculated values of R_g and ν for polymers from excluded volume polymer model fitting.

by fitting the SANS intensities to the excluded volume polymer model (Figures 2b-c and S4-7).[41] This analysis supports the previously observed similarities between the analogous copolymers, with similar Rg values for all SCNPs (3-5 nm, Figure 2c). Furthermore, the calculated scaling exponents support that FF-DMA (ν = 0.43) is more folded than F- and BAA-DMA (ν = 0.49 and 0.48 respectively), and these values are similar to those reported for covalently crosslinked SCNPs, while pDMA approximates a random coil (ν = 0.57).[1,42]

A comparison of the P(q) fits for polymer samples in dilute solution (2.5 mg/mL, lines in Figure 2b) to data obtained at the higher concentration required for NSE experiments (30 mg/mL, open symbols in Figure 2b) enabled the calculation of the concentration dependent structure factor [S(q, 30 mg/mL) = I(q, 30 mg/mL)/P(q, 2.5 mg/mL)], which is necessary to account for interparticle interactions when interpreting chain dynamics. A positive structure factor was observed for the SCNPs at low q (i.e., high length scales), indicating attractive interparticle interactions at high concentrations, whereas pDMA exhibited interparticle repulsion in the same q range. The calculated S(q) is small for all polymers in the q range observed by NSE ($0.14 > q > 0.04$), suggesting that the measured dynamics are minimally influenced by concentration dependent interparticle interactions.

Having established similar global structures between SCNPs, we sought to determine the effect of local structural differences on polymer dynamics using DLS and NSE. The NSE experiment was performed at the Neutron Spin Echo Spectrometer at SNS at Oak Ridge National Laboratory, SNS-NSE, BL-15.[43] For polymers in dilute solution, many dynamic modes, including center of mass diffusion, segmental relaxations, and internal dynamic modes, are active and observed in the NSE q-range as a decay in the dynamic structure factor [S(q,t)]. At each length scale observed by NSE, the decrease of the self-correlation function is faster for pDMA than FF-DMA and the analogous SCNPs, demonstrating the restricted mobility across length scales that results from chain folding (Figures 3a and S8-9). Furthermore, FF-DMA decays slower than the F-, and BAA- copolymers suggesting that β-sheet-like interactions impede chain mobility beyond the constraints of hydrogen-bonding and hydrophobicity (Figures 3b and S9). However, this analysis does not implicate which dynamic modes are more restricted within the FF-DMA copolymer.

To identify the origins of the dynamic differences between SCNPs formed with different local structures, we sought to isolate specific relaxation modes. In dilute solution, center of mass diffusion is expected to dominate polymer relaxations, especially at low q, where length scales exceed the dimensions of a single polymer. A linear fit of DLS diffusion measurements for polymer solutions ranging 1-30 mg/mL was used to extrapolate the center of mass diffusion coefficient (D_{CM}) at infinite dilution, representing the dynamics of a single chain without interparticle interactions (Figures 3c and S10). The measured D_{CM} values for the SCNPs and pDMA were similar, suggesting the reduction in radius due to folding has a minimal impact on translational motion, consistent with observations for low molecular weight SCNPs with covalent crosslinks.[28]

Extrapolation of the translational motion to shorter length scales measured by NSE, was calculated as

$$D_{CM}(q,c) = S(q,c) * D_{CM}(0) \qquad (1)$$

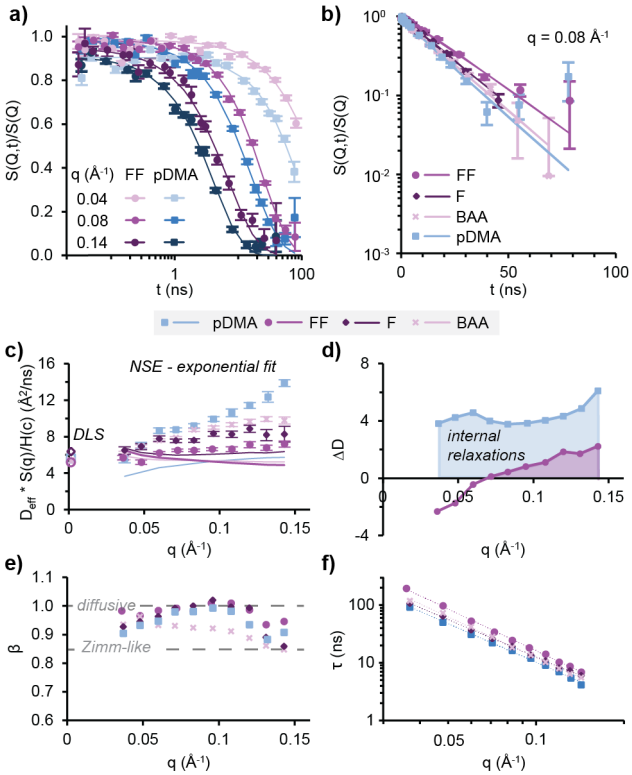

Figure 3. Dynamics of single-chain polymer nanoparticles (SCNPs) and pDMA. a) Neutron Spin Echo (NSE) plots for FF-DMA and pDMA at selected q values. Solid lines are fits of the stretched exponential function. b) NSE plots for SCNPs and pDMA at q = 0.08 Å^{-1}. Solid lines are fits of the stretched exponential function. c) D_{CM} (open symbols) and D_{eff} (filled symbols) for polymers. Solid lines are calculated $D_{CM}(q)$. d) Difference between D_{eff} and $D_{CM}(q)$ for FF- DMA and pDMA. e) β from stretched exponential fits of polymers. Dotted lines denote characteristic values for diffusive dynamics (top) and Zimm-like dynamics (bottom). f) Relaxation times (τ) from stretched exponential fits of each polymer. Dotted lines are power law fits.

and was used to determine the surplus of dynamic modes beyond D_{CM} at the measured length scales. The effective diffusion coefficient (D_{eff}), encompassing all of the chain dynamics, was calculated using the exponential function

$$S(q,t)/S(q,0) = A * \exp\left[-\left(t * D_{eff} * q^2\right)\right] \quad (2)$$

where A is a normalization coefficient and t is time. To compare the dynamics of the SCNPs and pDMA, D_{eff} was corrected for S(q) and the hydrodynamics factor (H(c); filled data points in Figure 3c).[29] H(c) was assumed constant as a function of q and was calculated for each polymer using

$$H(c) = D_{CM}(c) * S(q \rightarrow 0)/D_{CM}(0) \quad (3)$$

where $D_{CM}(c)$ was obtained from DLS (30 mg/mL).[25,28] As anticipated, D_{eff} agrees well with D_{CM} at low q, indicating that translational diffusion is the dominate relaxation mode observed at long length scales. However, additional relaxation modes are prevalent at shorter length scales, indicated by D_{eff} that are faster than D_{CM} at larger q values.

To illustrate the magnitude of these internal dynamics, the difference between D_{eff} and D_{CM} was calculated as $\Delta D = D_{eff} - D_{CM}$ (Figures 3d and S11). As compared to pDMA, FF-DMA and the analogous SCNPs have restricted internal dynamics resulting from their non-covalent intramolecular interactions. However, this analysis does not reveal the mechanism of these restrictions.

Additional information about the nature of the internal dynamics was obtained by fitting the NSE data to a stretched exponential function,

$$\frac{S(q,t)}{S(q,0)} = A * \exp\left[-\left(\frac{t}{\tau}\right)\right]^{\beta} \quad (4)$$

where A is a scaling factor, τ is the relaxation time, and β relates to the nature of the dynamics (Figures 3a-b and S9).[32] The obtained values of β indicate dynamic behavior between simple diffusion (β = 1) and that of a semi-flexible chain (Zimm-like relaxations; β ~ 0.85; Figure 3e).[32] These values are similar to those obtained for covalently cross-linked SCNPs.[28] Furthermore, the q dependence of

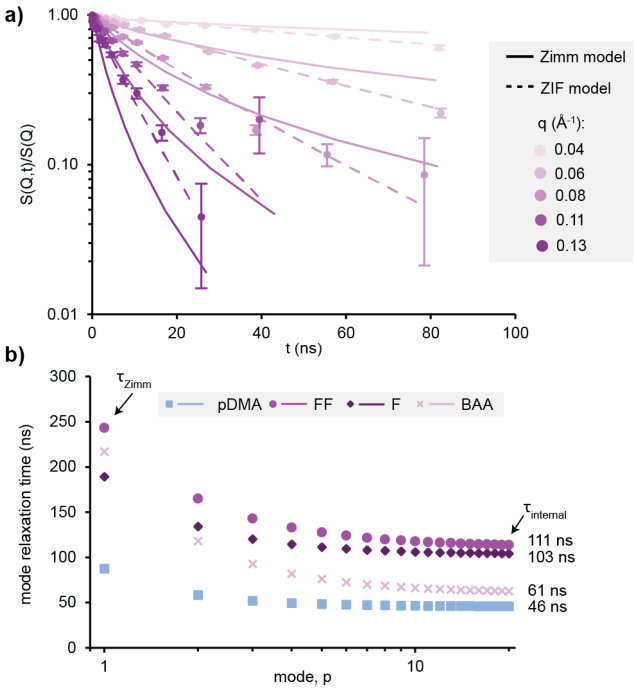

Figure 4. Zimm and Zimm with internal friction (ZIF) models applied to single-chain polymer nanoparticles and pDMA. a) Zimm model (solid lines) and ZIF model (dotted lines) of FF-DMA at selected q values. b) ZIF mode relaxation times for SCNPs and pDMA. Calculated internal friction values ($\tau_{internal}$) are listed to the right of each plot.

τ provides additional evidence to support the presence of internal relaxations in this system (Figure 3f). The correlation between q and τ for these polymers can be interpreted as the summation of local diffusive motions associated with different polymer segments.[44] Combined, these data implicate contributions from secondary relaxation modes, such as the rearrangement of chain segments, to the dynamics of FF-, F-, and BAA-DMA SCNPs in dilute solution.

To capture and quantify the complicated relaxation mechanisms that differentiate the dynamics of SCNPs with different local scale interactions, we sought to describe their dynamics with the Zimm and Zimm with internal friction (ZIF) models.[45–47] The Zimm model treats the polymer as a chain composed of N beads connected by ideal springs of length *l*, and it accounts for hydrodynamic interactions which impede motions as a function of solvent viscosity (η). These dynamics are described as

$$\frac{S(q,t)}{S(q,0)} = \frac{1}{N} e^{-q^2 D_{CM} t} \sum_{n,m}^{N} e^{-\frac{1}{6} q^2 B(n,m,t)} \qquad (6)$$

with the correlators

$$B(n,m,t) = |n-m|^{2\mu} l^2 + \sum_{p=1}^{N-1} A_p cos\left(\frac{\pi p n}{N}\right) cos\left(\frac{\pi p m}{N}\right)\left(1 - e^{-\frac{t}{\tau_p^{Zimm}}}\right) \qquad (7)$$

in terms of modes (p), where p = 0 corresponds to the center of mass diffusion of the chain and p > 0 relate to internal motions acting with decreasing amplitude. The characteristic time for each mode is described as

$$\tau_p^{Zimm} = \frac{\eta R_e^3}{\sqrt{(3\pi) k_B T)}} p^{-3\mu} \qquad (8)$$

with R_e as the end-to-end distance and the Boltzmann constant (k_B). The Zimm model was applied to the NSE data collected for each polymer using the Jscatter software with *l*, H(c), D_{CM}, and a y-axis scaling factor as fitting parameters.[48,49] The viscosity (η) of the buffered deuteroxide at 25 °C was estimated as 1.24 cP.[50] The Zimm model poorly described the experimental dynamics of the polymers at higher q and longer relaxation times ($\chi^2 > 10$; Figures 4a and S12-15 and Table S3). These results corroborate those from the stretched exponential fitting and implicate intrachain interactions that impede the motions of polymer segments.

We posited that the deviation from the Zimm predictions, especially at shorter length scales, reflected internal frictions resulting from the non-covalent interactions, as has been observed for both IDPs and covalently crosslinked SCNPs.[26,28] The ZIF model appends a mode independent time ($\tau_{internal}$) to each Zimm mode as $\tau_p^{ZIF} = \tau_p^{Zimm} + \tau_{internal}$.[47] Conceptually, $\tau_{internal}$ represents the impedance to chain dynamics from internal barriers, such as steric classes and intramolecular interactions. The ZIF model reproduces the experimental data well, reaffirming the impact of non-covalent interactions on polymer dynamics (Figures 4a and S12-15 and Table S4).

The relative effect of each non-covalent interaction to restrict chain mobility was assessed by comparing values of $\tau_{internal}$ (Figure 4b). The FF-DMA copolymer, which forms hydrogen-bonded β-sheet like fibrils, was found to have the largest dynamic impedance from

internal friction ($\tau_{internal}$ = 111 ns), followed closely by F-DMA that also forms hydrogen-bonds ($\tau_{internal}$ = 103 ns). However, BAA-DMA, which has a lower propensity for hydrogen-bonding, had significantly less internal friction ($\tau_{internal}$ = 61 ns). The dynamics the long DMA segments of the chain likely contribute minimally to the internal friction, as pDMA had a $\tau_{internal}$ = 46 ns. Despite their similar static structures, FF-, F-, and BAA-DMA SCNPs exhibit different dynamic behaviors as characterized by internal frictions, suggesting that the effects of non-covalent interactions compound as the interactions become more complex. These differences in local scale structures reflect the importance of hierarchical structure to mediate the properties of polymeric materials.

Conclusion

We have demonstrated the use of non-covalent interactions to mediate the dynamics of single-chain polymer nanoparticles (SCNPs) on a length scale relevant to target functions (pm-nm). Thus, we anticipate that these differences in dilute solution will aid in the rational design of functional biomimetic materials. Characterization of polymer structure spanning local and global length scales via SANS found that each SCNP in this study formed folded morphologies like those of intrinsically disordered proteins. Despite their similar structures, SCNPs in this study exhibited different dynamics as analyzed Neutron Spin Echo spectroscopy. Interpretation of the polymer dynamics using established Zimm and Zimm with internal friction (ZIF) models highlighted the importance of internal friction to describe the observed relaxations. Each SCNP displayed more internal friction than extended poly(dimethylacrylamide). Increasing internal barriers were observed with monomers capable of intramolecular hydrogen bonding (phenylalanine acrylamide) and β-sheet-like local structure (di(phenylalanine) acrylamide), resulting in slower dynamics. Collectively, these data highlight the additive role of each non-covalent interaction to induce structure and constrain chain mobility. Leveraging this control of polymer dynamics through synthetic design will facilitate the development of biomimetic materials with increasingly complex functions, such as sensors and catalysts that rival the capabilities of native proteins.

ASSOCIATED CONTENT

Supporting information containing synthetic procedures, experimental details, supplemental tables, and figures including DLS, CD, SEC, SANS, and NSE characterization is available.

AUTHOR INFORMATION

Corresponding Author

* Abigail S. Knight (aknight@unc.edu)

Author Contributions

[a]PDB and LRS contributed equally to this manuscript.

ACKNOWLEDGMENT

This work was supported by the U.S. Department of Energy, Office of Science, Office of Basic Energy Sciences under Award Number DE-SC0021295. P.D.B. acknowledges support from the National Institute of General Medical Sciences of the National Institutes of Health under Award Number T32GM135122. This research used resources at the Spallation Neutron Source, a DOE Office of Science User Facility operated by the Oak Ridge National Laboratory. We acknowledge the UNC Macromolecular Interactions Facility (CD and DLS; supported by the National Cancer Institute of the National Institutes of Health under award number P30CA016086) and the UNC NMR Core Laboratory (supported by the National Science Foundation Award Number CHE-1828183). Model protein SAXS and SANS data were acquired from the Small Angle Scattering Biological Data Bank.[51] Finally, we thank Drs. Carrie Gao and Mary Odom for their assistance with SANS and NSE measurements respectively.

ABBREVIATIONS

SCNP, single-chain polymer nanoparticle; FF, di(phenylalanine) acrylamide; F, phenylalanine acrylamide; BAA, benzyl acrylamide; pDMA, poly(dimethylacrylamide); ZIF, Zimm with internal Friction; CD, circular dichroism; DLS, dynamic light scattering; RAFT, reversible addition-fragmentation transfer; R_g, radius of gyration, SANS, Small Angle Neutron Scattering; NSE, Neutron Spin Echo; IDP, intrinsically disordered protein.

REFERENCES

(1) Pomposo, J. A.; Perez-Baena, I.; Lo Verso, F.; Moreno, A. J.; Arbe, A.; Colmenero, J. How Far Are Single-Chain Polymer Nanoparticles in Solution from the Globular State? *ACS Macro Letters* **2014**, *3* (8), 767–772. https://doi.org/10.1021/mz500354q.

(2) Lyon, C. K.; Prasher, A.; Hanlon, A. M.; Tuten, B. T.; Tooley, C. A.; Frank, P. G.; Berda, E. B. A Brief User's Guide to Single-Chain Nanoparticles. *Polymer Chemistry* **2015**, *6* (2), 181–197. https://doi.org/10.1039/c4py01217h.

(3) Barbee, M. H.; Wright, Z. M.; Allen, B. P.; Taylor, H. F.; Patteson, E. F.; Knight, A. S. Protein-Mimetic Self-Assembly with Synthetic Macromolecules. *Macromolecules* **2021**, acs.macromol.0c02826. https://doi.org/10.1021/acs.macromol.0c02826.

(4) Matsumoto, K.; Terashima, T.; Sugita, T.; Takenaka, M.; Sawamoto, M. Amphiphilic Random Copolymers with Hydrophobic/Hydrogen-Bonding Urea Pendants: Self-Folding Polymers in Aqueous and Organic Media. *Macromolecules* **2016**, *49* (20), 7917–7927. https://doi.org/10.1021/acs.macromol.6b01702.

(5) Stals, P. J. M.; Gillissen, M. A. J.; Paffen, T. F. E.; De Greef, T. F. A.; Lindner, P.; Meijer, E. W.; Palmans, A. R. A.; Voets, I. K. Folding Polymers with Pendant Hydrogen Bonding Motifs in Water: The Effect of Polymer Length and Concentration on the

Shape and Size of Single-Chain Polymeric Nanoparticles. *Macromolecules* **2014**, *47* (9), 2947–2954. https://doi.org/10.1021/MA500273G/SUPPL_FILE/MA500273G_SI_001.PDF.

(6) Kodura, D.; Houck, H. A.; Bloesser, F. R.; Goldmann, A. S.; Prez, F. E. D.; Frisch, H.; Barner-Kowollik, C. Light-Fueled Dynamic Covalent Crosslinking of Single Polymer Chains in Non-Equilibrium States. *Chem. Sci.* **2021**, *12* (4), 1302–1310. https://doi.org/10.1039/D0SC05818A.

(7) He, J.; Tremblay, L.; Lacelle, S.; Zhao, Y. Preparation of Polymer Single Chain Nanoparticles Using Intramolecular Photodimerization of Coumarin. *Soft Matter* **2011**, *7* (6), 2380–2386. https://doi.org/10.1039/C0SM01383H.

(8) Tuten, B. T.; Chao, D.; Lyon, C. K.; Berda, E. B. Single-Chain Polymer Nanoparticles via Reversible Disulfide Bridges. *Polymer Chemistry* **2012**, *3* (11), 3068–3071. https://doi.org/10.1039/C2PY20308A.

(9) Reith, M. A.; Kardas, S.; Mertens, C.; Fossépré, M.; Surin, M.; Steinkoenig, J.; Du Prez, F. E. Using Nickel to Fold Discrete Synthetic Macromolecules into Single-Chain Nanoparticles. *Polymer Chemistry* **2021**, *12* (34), 4924–4933. https://doi.org/10.1039/D1PY00229E.

(10) Berkovich, I.; Mavila, S.; Iliashevsky, O.; Kozuch, S.; Lemcoff, N. G. Single-Chain Polybutadiene Organometallic Nanoparticles: An Experimental and Theoretical Study. *Chemical Science* **2016**, *7* (3), 1773–1778. https://doi.org/10.1039/C5SC04535E.

(11) Sanchez-Sanchez, A.; Arbe, A.; Colmenero, J.; Pomposo, J. A. Metallo-Folded Single-Chain Nanoparticles with Catalytic Selectivity. *ACS Macro Letters* **2014**, *3* (5), 439–443. https://doi.org/10.1021/MZ5001477/SUPPL_FILE/MZ5001477_SI_001.PDF.

(12) Wijker, S.; Palmans, A. R. A. Protein-Inspired Control over Synthetic Polymer Folding for Structured Functional Nanoparticles in Water. *ChemPlusChem* **2023**, *88* (7), e202300260. https://doi.org/10.1002/cplu.202300260.

(13) Verde-Sesto, E.; Arbe, A.; Moreno, A. J.; Cangialosi, D.; Alegría, A.; Colmenero, J.; Pomposo, J. A. Single-Chain Nanoparticles: Opportunities Provided by Internal and External Confinement. *Materials Horizons* **2020**, *7* (9), 2292–2313. https://doi.org/10.1039/D0MH00846J.

(14) Rubio-Cervilla, J.; González, E.; Pomposo, J. A. Advances in Single-Chain Nanoparticles for Catalysis Applications. *Nanomaterials* **2017**, *7* (10). https://doi.org/10.3390/NANO7100341.

(15) Chen, J.; Wang, J.; Bai, Y.; Li, K.; Garcia, E. S.; Ferguson, A. L.; Zimmerman, S. C. Enzyme-like Click Catalysis by a Copper-Containing Single-Chain Nanoparticle. *J. Am. Chem. Soc.* **2018**, *140* (42), 13695–13702. https://doi.org/10.1021/jacs.8b06875.

(16) Sanders, M. A.; Chittari, S. S.; Sherman, N.; Foley, J. R.; Knight, A. S. Versatile Triphenylphosphine-Containing Polymeric Catalysts and Elucidation of Structure–Function Relationships. *J. Am. Chem. Soc.* **2023**. https://doi.org/10.1021/jacs.3c01092.

(17) Dykeman-Bermingham, P. A.; Bogen, M. P.; Chittari, S. S.; Grizzard, S. F.; Knight, A. S. Tailoring Hierarchical Structure and Rare Earth Affinity of Compositionally Identical Polymers via Sequence Control. *J. Am. Chem. Soc.* **2024**. https://doi.org/10.1021/jacs.4c00440.

(18) Spicuzza, M.; Gaikwad, S. P.; Huss, S.; Lee, A. A.; Craescu, C. V.; Griggs, A.; Joseph, J.; Puthenpurayil, M.; Lin, W.; Matarazzo, C.; Baldwin, S.; Perez, V.; Rodriguez-Acevedo, D. A.; Swierk, J. R.; Elacqua, E. Visible-Light-Mediated Diels–Alder Reactions under Single-Chain Polymer Confinement: Investigating the Role of the Crosslinking Moiety on Catalyst Activity. *Polym. Chem.* **2024**. https://doi.org/10.1039/D4PY00282B.

(19) Engelke, J.; Tuten, B. T.; Schweins, R.; Komber, H.; Barner, L.; Plüschke, L.; Barner-Kowollik, C.; Lederer, A. An In-Depth Analysis Approach Enabling Precision Single Chain Nanoparticle Design. *Polym. Chem.* **2020**, *11* (41), 6559–6578. https://doi.org/10.1039/D0PY01045F.

(20) Henzler-Wildman, K.; Kern, D. Dynamic Personalities of Proteins. *Nature* **2007**, *450* (7172), 964–972. https://doi.org/10.1038/nature06522.

(21) Heatley, F. Polymers: Relaxation and Dynamics of Synthetic Polymers in Solution. *Encyclopedia of Magnetic Resonance* **2007**. https://doi.org/10.1002/9780470034590.EMRSTM0408.

(22) Wei, Y.; Hore, M. J. A. Characterizing Polymer Structure with Small-Angle Neutron Scattering: A Tutorial. *Journal of Applied Physics* **2021**, *129* (17), 171101. https://doi.org/10.1063/5.0045841.

(23) Liao, S.; Wei, L.; Abriata, L. A.; Stellacci, F. Control and Characterization of the Compactness of Single-Chain Nanoparticles. *Macromolecules* **2021**, acs.macromol.1c02071. https://doi.org/10.1021/ACS.MACROMOL.1C02071.

(24) Nagao, M.; Miura, Y. Correlation between Self-Folding Behavior of Amphiphilic Polymers and Their Molecular Flexibility. *ACS Macro Lett.* **2023**, 733–737. https://doi.org/10.1021/acsmacrolett.3c00182.

(25) Stadler, A. M.; Stingaciu, L.; Radulescu, A.; Holderer, O.; Monkenbusch, M.; Biehl, R.; Richter, D. Internal Nanosecond Dynamics in the Intrinsically Disordered Myelin Basic Protein. *Journal of the American Chemical Society* **2014**, *136* (19), 6987–6994. https://doi.org/10.1021/JA502343B.

(26) Stingaciu, L. R.; Biehl, R.; Changwoo, D.; Richter, D.; Stadler, A. M. Reduced Internal Friction by Osmolyte Interaction in Intrinsically Disordered Myelin Basic Protein. *The journal of physical chemistry letters* **2020**, *11* (1), 292–296. https://doi.org/10.1021/ACS.JPCLETT.9B03001.

(27) Buvalaia, E.; Kruteva, M.; Hoffmann, I.; Radulescu, A.; Förster, S.; Biehl, R. Interchain Hydrodynamic Interaction and Internal Friction of Polyelectrolytes. *ACS Macro Lett.* **2023**, *12* (9), 1218–1223. https://doi.org/10.1021/acsmacrolett.3c00409.

(28) González-Burgos, M.; Asenjo-Sanz, I.; Pomposo, J. A.; Radulescu, A.; Ivanova, O.; Pasini, S.; Arbe, A.; Colmenero, J. Structure and Dynamics of Irreversible Single-Chain Nanoparticles in Dilute Solution. A Neutron Scattering Investigation. *Macromolecules* **2020**, *53* (18), 8068–8082. https://doi.org/10.1021/ACS.MACROMOL.0C01451.

(29) Arbe, A.; Pomposo, J. A.; Moreno, A. J.; LoVerso, F.; González-Burgos, M.; Asenjo-Sanz, I.; Iturrospe, A.; Radulescu, A.; Ivanova, O.; Colmenero, J. Structure and Dynamics of Single-Chain Nano-Particles in Solution. *Polymer* **2016**, *105*, 532–544. https://doi.org/10.1016/J.POLYMER.2016.07.059.

(30) Warren, J. L.; Dykeman-Bermingham, P. A.; Knight, A. S. Controlling Amphiphilic Polymer Folding beyond the Primary Structure with Protein-Mimetic Di(Phenylalanine). *J. Am. Chem. Soc.* **2021**, *143* (33), 13228–13234. https://doi.org/10.1021/jacs.1c05659.

(31) Farazi, S.; Stenzel, M. H.; Chapman, R. Confinement of Folding Motifs within Central Blocks Improves Single Chain Polymer Nanoparticle Folding. *Polym. Chem.* **2024**, *15* (4), 332–340. https://doi.org/10.1039/D3PY01166F.

(32) Richter, D.; Monkenbusch, M.; Arbe, A.; Colmenero, J. Neutron Spin Echo in Polymer Systems. In *Neutron Spin Echo in Polymer Systems*; Richter, D., Monkenbusch, M., Arbe, A., Colmenero, J., Eds.; Springer: Berlin, Heidelberg, 2005; pp 1–221. https://doi.org/10.1007/b106578.

(33) Mishra, A.; Chauhan, V. S. Probing the Role of Aromaticity in the Design of Dipeptide Based Nanostructures. *Nanoscale* **2011**, *3* (3), 945–949. https://doi.org/10.1039/c0nr00691b.

(34) Zhao, J. K.; Gao, C. Y.; Liu, D. The Extended Q-Range Small-Angle Neutron Scattering Diffractometer at the SNS. *J Appl Cryst* **2010**, *43* (5), 1068–1077. https://doi.org/10.1107/S002188981002217X.

(35) Burger, V. M.; Arenas, D. J.; Stultz, C. M. A Structure-Free Method for Quantifying Conformational Flexibility in Proteins. *Sci Rep* **2016**, *6* (1), 29040. https://doi.org/10.1038/srep29040.

(36) Trewhella, J.; Vachette, P.; Bierma, J.; Blanchet, C.; Brookes, E.; Chakravarthy, S.; Chatzimagas, L.; Cleveland, T. E.; Cowieson, N.; Crossett, B.; Duff, A. P.; Franke, D.; Gabel, F.; Gillilan, R. E.; Graewert, M.; Grishaev, A.; Guss, J. M.; Hammel, M.; Hopkins, J.; Huang, Q.; Hub, J. S.; Hura, G. L.; Irving, T. C.; Jeffries, C. M.; Jeong, C.; Kirby, N.; Krueger, S.; Martel, A.; Matsui, T.; Li, N.; Pérez, J.; Porcar, L.; Prangé, T.; Rajkovic, I.; Rocco, M.; Rosenberg, D. J.; Ryan, T. M.; Seifert, S.; Sekiguchi, H.; Svergun, D.; Teixeira, S.; Thureau, A.; Weiss, T. M.; Whitten, A. E.; Wood, K.; Zuo, X. A Round-Robin Approach Provides a Detailed Assessment of Biomolecular Small-Angle Scattering Data Reproducibility and Yields Consensus Curves for Benchmarking. *Acta Cryst D* **2022**, *78* (11), 1315–1336. https://doi.org/10.1107/S2059798322009184.

(37) González-Foutel, N. S.; Glavina, J.; Borcherds, W. M.; Safranchik, M.; Barrera-Vilarmau, S.; Sagar, A.; Estaña, A.; Barozet, A.; Garrone, N. A.; Fernandez-Ballester, G.; Blanes-Mira, C.; Sánchez, I. E.; de Prat-Gay, G.; Cortés, J.; Bernadó, P.; Pappu, R. V.; Holehouse, A. S.; Daughdrill, G. W.; Chemes, L. B. Conformational Buffering Underlies Functional Selection in Intrinsically Disordered Protein Regions. *Nat Struct Mol Biol* **2022**, *29* (8), 781–790. https://doi.org/10.1038/s41594-022-00811-w.

(38) Kikhney, A. G.; Svergun, D. I. A Practical Guide to Small Angle X-Ray Scattering (SAXS) of Flexible and Intrinsically Disordered Proteins. *FEBS Letters* **2015**, *589* (19, Part A), 2570–2577. https://doi.org/10.1016/j.febslet.2015.08.027.

(39) Receveur-Bréchot, V.; Durand, D. How Random Are Intrinsically Disordered Proteins? A Small Angle Scattering Perspective. *Curr Protein Pept Sci* **2012**, *13* (1), 55–75. https://doi.org/10.2174/138920312799277901.

(40) Upadhya, R.; Murthy, N. S.; Hoop, C. L.; Kosuri, S.; Nanda, V.; Kohn, J.; Baum, J.; Gormley, A. J. PET-RAFT and SAXS: High Throughput Tools to Study Compactness and Flexibility of Single-Chain Polymer Nanoparticles. *Macromolecules* **2019**, *52* (21), 8295–8304. https://doi.org/10.1021/acs.macromol.9b01923.

(41) Hammouda, B. SANS from Homogeneous Polymer Mixtures: A Unified Overview. In *Polymer Characteristics*; Advances in Polymer Science; Springer: Berlin, Heidelberg, 1993; pp 87–133. https://doi.org/10.1007/BFb0025862.

(42) Flory, P. J. The Configuration of Real Polymer Chains. *The Journal of Chemical Physics* **1949**, *17* (3), 303–310. https://doi.org/10.1063/1.1747243.

(43) Ohl, M.; Monkenbusch, M.; Arend, N.; Kozielewski, T.; Vehres, G.; Tiemann, C.; Butzek, M.; Soltner, H.; Giesen, U.; Achten, R.; Stelzer, H.; Lindenau, B.; Budwig, A.; Kleines, H.; Drochner, M.; Kaemmerling, P.; Wagener, M.; Möller, R.; Iverson, E. B.; Sharp, M.; Richter, D. The Spin-Echo Spectrometer at the Spallation Neutron Source (SNS). *Nuclear Instruments and Methods in Physics Research Section A: Accelerators, Spectrometers, Detectors and Associated Equipment* **2012**, *696*, 85–99. https://doi.org/10.1016/j.nima.2012.08.059.

(44) Arbe, A.; Colmenero, J.; Monkenbusch, M.; Richter, D. Dynamics of Glass-Forming Polymers: "Homogeneous" versus "Heterogeneous" Scenario. *Phys. Rev. Lett.* **1998**, *81* (3), 590–593. https://doi.org/10.1103/PhysRevLett.81.590.

(45) Zimm, B. H. Dynamics of Polymer Molecules in Dilute Solution: Viscoelasticity, Flow Birefringence and Dielectric Loss. *The Journal of Chemical Physics* **1956**, *24* (2), 269–278. https://doi.org/10.1063/1.1742462.

(46) Rouse, P. E., Jr. A Theory of the Linear Viscoelastic Properties of Dilute Solutions of Coiling Polymers. *The Journal of Chemical Physics* **1953**, *21* (7), 1272–1280. https://doi.org/10.1063/1.1699180.

(47) Arbe, A.; Monkenbusch, M.; Stellbrink, J.; Richter, D.; Farago, B.; Almdal, K.; Faust, R. Origin of Internal Viscosity Effects in Flexible Polymers: A Comparative Neutron Spin-Echo and Light Scattering Study on Poly(Dimethylsiloxane) and Polyisobutylene. *Macromolecules* **2001**, *34* (5), 1281–1290. https://doi.org/10.1021/MA001628X.

(48) Biehl, R. Jscatter, a Program for Evaluation and Analysis of Experimental Data. *PLOS ONE* **2019**, *14* (6), e0218789. https://doi.org/10.1371/journal.pone.0218789.

(49) Ralf, B. Jscatter, a Program for Evaluation and Analysis of Experimental Data, 2019. https://doi.org/10.5281/zenodo.3334712.

(50) Hardy, R. C.; Cottington, R. L. Viscosity of Deuterium Oxide and Water in the Range 5 °C to 125 °C. *Journal of Research of the National Bureau of Standards* **1949**, *42*, 573–578. https://doi.org/10.6028/jres.042.049.

(51) Valentini, E.; Kikhney, A. G.; Previtali, G.; Jeffries, C. M.; Svergun, D. I. SASBDB, a Repository for Biological Small-Angle Scattering Data. *Nucleic Acids Research* **2015**, *43* (D1), D357–D363. https://doi.org/10.1093/nar/gku1047.